RESEARCH ARTICLE

INNATE IMMUNITY

Structural and biochemical basis for induced self-propagation of NLRC4

Zehan Hu,^{1*} Qiang Zhou,^{2*} Chenlu Zhang,^{1*} Shilong Fan,¹ Wei Cheng,³ Yue Zhao,⁴ Feng Shao,⁴ Hong-Wei Wang,¹ Sen-Fang Sui,²† Jijie Chai¹†

Responding to stimuli, nucleotide-binding domain and leucine-rich repeat—containing proteins (NLRs) oligomerize into multiprotein complexes, termed inflammasomes, mediating innate immunity. Recognition of bacterial pathogens by NLR apoptosis inhibitory proteins (NAIPs) induces NLR family CARD domain—containing protein 4 (NLRC4) activation and formation of NAIP-NLRC4 inflammasomes. The wheel-like structure of a PrgJ-NAIP2-NLRC4 complex determined by cryogenic electron microscopy at 6.6 angstrom reveals that NLRC4 activation involves substantial structural reorganization that creates one oligomerization surface (catalytic surface). Once activated, NLRC4 uses this surface to catalyze the activation of an inactive NLRC4, self-propagating its active conformation to form the wheel-like architecture. NAIP proteins possess a catalytic surface matching the other oligomerization surface (receptor surface) of NLRC4 but not those of their own, ensuring that one NAIP is sufficient to initiate NLRC4 oligomerization.

ucleotide-binding domain (NBD)- and leucine-rich repeat (LRR)-containing proteins (NLRs) are critical for the cytosolic immunosurveillance system of mammals (1-4). Dysregulation of NLR function is associated with several human diseases (5-8). NLRs are pattern recognition receptors that recognize pathogen-associated molecular patterns (PAMPs) or host-derived danger components, resulting in NLR activation and oligomerization (1, 4). The oligomerized NLRs then recruit procaspase-1 (pro-Casp1) either directly or through the adaptor protein apoptosis-associated speck-like protein containing CARD (caspase activation and recruitment domain) (ASC), forming inflammasomes that catalyze Casp-1 activation (1, 9). Once activated, Casp-1 proteolytically processes prointerleukin 1\beta (pro-IL-1\beta) and pro-IL-18 to initiate host innate immune responses.

NLR proteins contain a varied N-terminal domain such as CARD or pyrin domain (PYD), a central nucleotide binding and oligomerization domain (NOD), and a C-terminal LRR domain (4). The NOD module, containing an NBD and a helical domain 1 (HD1) followed by a wingedhelical domain (WHD) (10), is an adenosine

¹Ministry of Education Key Laboratory of Protein Science, Center for Structural Biology, School of Life Sciences, Tsinghua-Peking Joint Center for Life Sciences, Tsinghua University, Beijing 100084, China. ²State Key Laboratory of Biomembrane and Membrane Biotechnology, Center for Structural Biology, School of Life Sciences, Tsinghua University, Beijing 100084, China. ³Division of Respiratory and Critical Care Medicine, State Key Laboratory of Biotherapy, West China Hospital, Sichuan University, and Collaborative Innovation Center of Biotherapy, Chengdu, China. ⁴National Institute of Biological Sciences, Beijing 102206, China.

**These authors contributed equally to this work. †Corresponding author. E-mail: chaijj@tsinghua.edu.cn (J.C.); suisf@mail.tsinghua.edu.cn (S.F.S.)

diphosphate-adenosine triphosphate binding motif conserved in the apoptotic proteins Apaf-1 and CED-4 (*II*). NLRs are maintained in an autoinhibited state by their C-terminal LRR domains (*12, 13*). Recent studies support a unified model of NLR activation in which ligand-induced clustering of PYD from an NLR [or absent in melanoma 2 (AIM2)] serves to nucleate the ASC^{PYD} filament for Casp-1 polymerization and activation (*14, 15*).

NLRC4 inflammasomes are activated by bacterial pathogens carrying flagellin or the components of type III secretion system (T3SS) (16-23). Specificity of the NLRC4 inflammasomes for different bacterial ligands is dictated by NLR apoptosis inhibitory proteins (NAIPs) (24, 25) that contain three baculoviral inhibitor of apoptosis (IAP) repeat (BIR) domains at their N-terminal sides. In mice, direct recognition of the bacterial flagellin and the T3SS rod protein PrgJ is mediated by NAIP5/6 and NAIP2, respectively (24, 25). The structural determinants for recognition of the two bacterial PAMPs lie in the NOD module of a NAIP protein (26). Ligand binding induces NAIP interaction with NLRC4, followed by oligomerization of their complex (24, 25). Assembly of flagellin-NAIP5-NLRC4 inflammasomes was proposed to follow a sequential manner (27), but evidence for this model is lacking.

Results

The wheel-like structure of a PrgJ-NAIP2-NLRC4 complex revealed by cryo-EM

A protein complex composed of PrgJ, NAIP2, and full-length NLRC4 (NLRC4^{FL}, fig. S1A) but not a CARD-truncated NLRC4 (residues 90 to 1024, NLRC4^{ΔCARD}) (fig. S1B) contained double-ring structures as revealed by cryogenic electron mi-

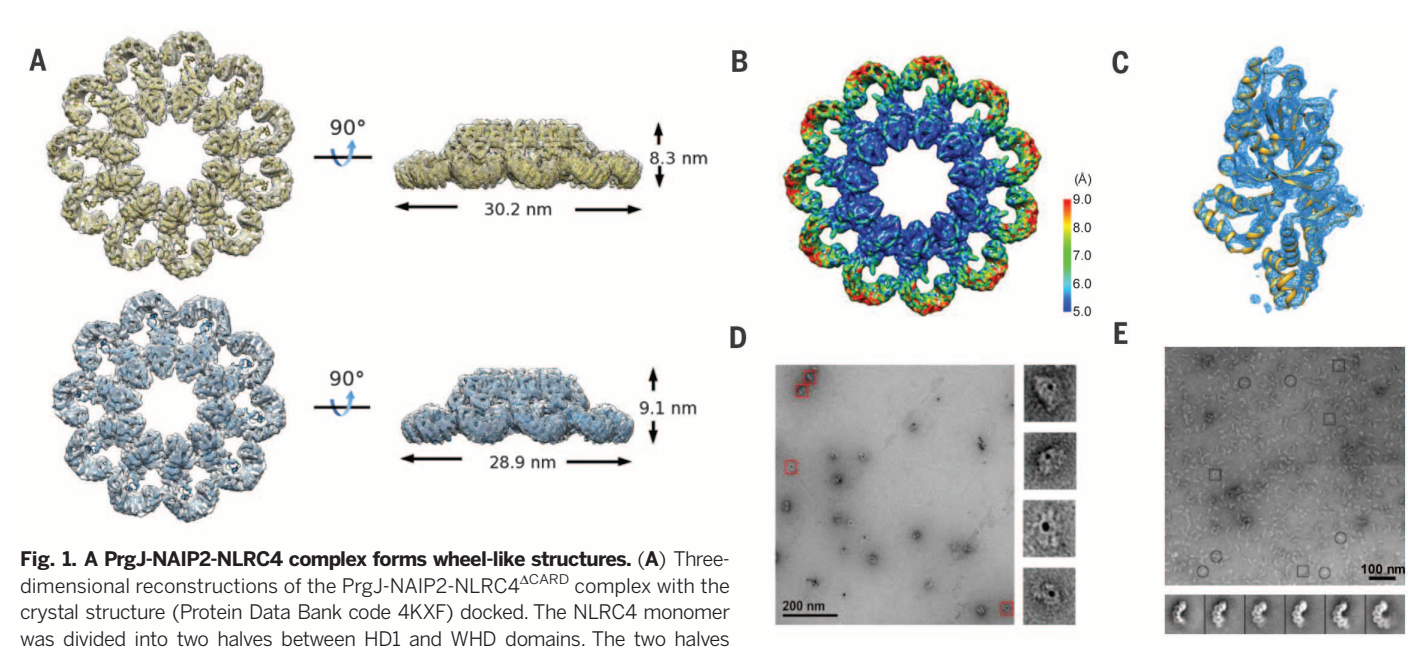
croscopy (cryo-EM) (figs. S2A and S3A), indicating that the double-ring structures are mediated by the CARD of NLRC4. Two-dimensional (2D) class averages of the latter complex revealed particles featuring wheel-like structures containing mainly 11, some 10 (fig. S2A, bottom panel), and a small fraction of 12 protomers, and multilayer structures (fig. S2, B and C). The wheel-like architectures are further supported by comparison of the single-layer side-view averages with their mirrored images (fig. S2D).

Intriguingly, particles of the NLRC4^{FL}-containing complex mainly contained 11 and 12 protomers (fig. S3, A to F, and table S1), similar to those purified from mammalian cells (27). In the 2D class averages without imposing any symmetry, the 10, 11, or 12 protomers within one particle are highly similar (figs. S2A and S3A), suggesting that NAIP2 and NLRC4 have a conserved structure, as evidenced by sequence alignment of NLR proteins (fig. S4). Further supporting their conserved structures, the 3D reconstructions of the 11- and 10-protomer without imposing any symmetry revealed wheel-like structures with pseudosymmetry (fig. S2E). We thus performed 3D reconstruction refinement of the two types of complexes with c11 or c10 symmetry averaging. The resulting cryo-EM maps (Fig. 1A) had an overall resolution of 6.6 Å for the 11-protomer (NLRC4 $^{\Delta CARD}\text{-containing complex)}$ and 6.7 Å for the 10-protomer complex (fig. S2, F to K, and table S1). These two types of complexes slightly differ in diameter and height (Fig. 1A). Separate rigid-body fitting of the NBD-HD1 module and its following C-terminal segment (WHD-HD2-LRR) from the inactive NLRC4 (13) into the EM volumes demonstrated a high compatibility with the 3D reconstructions (Fig. 1A). Local resolution analysis indicated that the inner part of the 11-protomer wheel-like structure was of significantly higher resolution (5.5 Å) (Fig. 1B), allowing an easy assignment of secondary structure elements of the NOD module (Fig. 1C).

Some registry errors will be present in our models, as NAIP2 was approximated to NLRC4, but the models are sufficient to characterize domain organization and interactions between secondary structural elements, the main focuses of our current study. We limit our discussions to the I1-protomer model of the PrgJ-NAIP2-NLRC4^{ΔCARD} complex that is nearly identical with that of the I1-protomer PrgJ-NAIP2-NLRC4^{FL} complex (fig. S3G).

A single NAIP2 initiates progressive assembly of the wheel-like structure

To determine the stoichiometry of the PrgJ-NAIP2-NLRC4^{ACARD} complex, we performed Ni-NTA-nanogold labeling EM (against the N-terminally His-tagged NAIP2) for the oligomerized complex eluted at higher molecular weights (fig. S1C, bottom panel). The results showed that each single particle of the complex was bound by one gold particle (Fig. 1D and fig. S5A), suggesting that the complex contained one NAIP2 molecule. Ni-NTA-nanogold labeling EM against the



were joined together again with Modeller after rigid-body docking into the cryo-EM density map by UCSF Chimera. (Top) the 11-protomer complex; (bottom) the 10-protomer complex. (B) The local resolution of cryo-EM density map of the PrgJ-NAIP2-NLRC4^{ACARD} complex with c11 symmetry. (C) Finally refined cryo-EM density map surrounding the NOD module of NLRC4. (D) Ni-NTA-nanogold labeling (5.0 nm) of the N-terminally His-tagged NAIP2 in complex with PrgJ and NLRC4^{ACARD} eluted at positions of higher molecular weights (see fig. S1C). On the left is a representative negative-stain micrograph of the nanogoldlabeled complex. Particles highlighted in red squares are shown in the insets. (E) Partially oligomerized structures of the PrgJ-NAIP2-NLRC4^{ΔCARD} complex eluted at lower molecular weights (see fig. S1C). (Top) A representative negative-stain micrograph of the PrgJ-NAIP2-NLRC4^{ΔCARD} complex. (Bottom) Representative 2D class averages of PrgJ-NAIP2-NLRC4^{ΔCARD} particles.

N-terminally His-tagged PrgJ for the same complex gave a similar result (fig. S5B). Consistently, gel filtration analysis showed that PrgJ-NAIP2-NLRC4 $^{\rm FL}$ and PrgJ-NAIP2-NLRC4^{ΔCARD} were substoichiometric complexes (fig. S1C).

PrgJ-NAIP2-NLRC4 $^{\Delta CARD}$ eluted at the positions of lower molecular weights (fig. S1C, bottom panel) formed unclosed and twisted structures with variable sizes (Fig. 1E). Owing to the absence of pseudo-symmetry in these complexes, the 2D classification tends to align the open ends of the particles for maximal overlap and thus likely reveals subtle structural differences between NAIP2 and NLRC4 if the single NAIP2 in one structure is not randomly positioned. Indeed, for each particle type the protomer at one end appears different from the remaining copies in the 2D class averages (Fig. 1E, bottom panel), suggesting that it corresponds to NAIP2. This agrees with the concept that assembly of the NAIP-NLRC4 inflammasomes starts with ligand-induced activation of a NAIP molecule (24, 25). Further supporting our conclusion, a nanogold-labeling EM (against NAIP2) study showed that a single nanogold particle bound to one partially oligomerized complex particle (fig. S5C). This conclusion is also in line with our observation that NAIP2 and NAIP5, although highly conserved in their sequences, failed to coexist in the same single-ring structure (fig. S6).

NOD-mediated formation of the wheel-like structure of PrgJ-NAIP2-NLRC4^{△CARD}

One side of the NOD module from each protomer packs against the opposite side of the

NOD from the adjacent protomer in an invariant fashion (Fig. 2, A and B), providing the major protomer-protomer interactions that stabilize the wheel-like structure. Two adjacent LRRs contact each other largely through complementary charged surfaces (fig. S7). The wheellike architecture (Fig. 2A) is reminiscent of the structures of Apaf-1 (28), DARK (29, 30) and CED-4 (31) apoptosomes. However, marked differences exist between NLRC4 and Apaf-1 in oligomeric assembly (fig. S8, A and B). Apaf-1 and DARK oligomerization is predominantly mediated by the structural elements from NBD and HD1 (28, 30). By contrast, the WHD of NLRC4 is also involved in the formation of a lateral dimer besides NBD and HD1 (Fig. 2B).

Structural remodeling creates one oligomerization surface during **NLRC4** activation

Structure comparison revealed that NLRC4 undergoes striking structural remodeling during activation, with WHD-HD2-LRR rotating largely as a rigid body ~90 degrees around the hinge region (residues 354 to 356) between HD1 and WHD (Fig. 2C and figs. S9 and S10). One dimeric surface, formed by structural elements from NBD and HD1, is largely exposed in the inactive NLRC4 (Fig. 2D and fig. S11, right panel). This surface (hereafter called receptor surface) is preformed, because NBD and HD1 undergo little change relative to each other during activation. Interaction of the inactive NLRC4 with an activated NLRC4 is sterically hindered by the C-terminal end of α15 (labeled in red) from the WHD of the inactive NLRC4 (Fig. 2D), located immediately after the hinge region (Fig. 2C). By contrast, the LRR domain is positioned by the other oligomeric surface (hereafter called catalytic surface) in the inactive NLRC4 and completely overlaps with its neighboring NLRC4 protomer from a lateral dimer (Fig. 2E and fig. S11, left panel). In further contrast with the receptor surface, half of the catalytic surface is composed of structural elements from the WHD (Fig. 2E), indicating that this oligomerization surface is activation-created and can be fully formed only after structural reorganization of NLRC4 during activation. By comparison, both of the two oligomeric surfaces of Apaf-1 are preexistent in an inactive Apaf-1 (28, 32) (fig. S8C).

The catalytic surface initiates **NLRC4** autoactivation

Formation of the unclosed structures (Fig. 1E) starting with NAIP2 indicates that their assembly is a unidirectional process. The propagation direction of these structures can be unambiguously determined by the observation that the C-terminal portion of LRR domain from each protomer is located at the same side as the catalytic surface of NLRC4 (Figs. 1E and 2B). These results strongly suggest that an activated NLRC4 uses the catalytic surface for interaction with and activation of an inactive NLRC4 (Fig. 3, A and B), leading to progressive intermolecular autoactivation of NLRC4. On the other hand, the equivalent positioning of NAIP2 to NLRC4 in the 2D class averages (Fig. 1E) suggests that the receptor surface of NLRC4 contacts NAIP2. Fully supporting

23 OCTOBER 2015 • VOL 350 ISSUE 6259

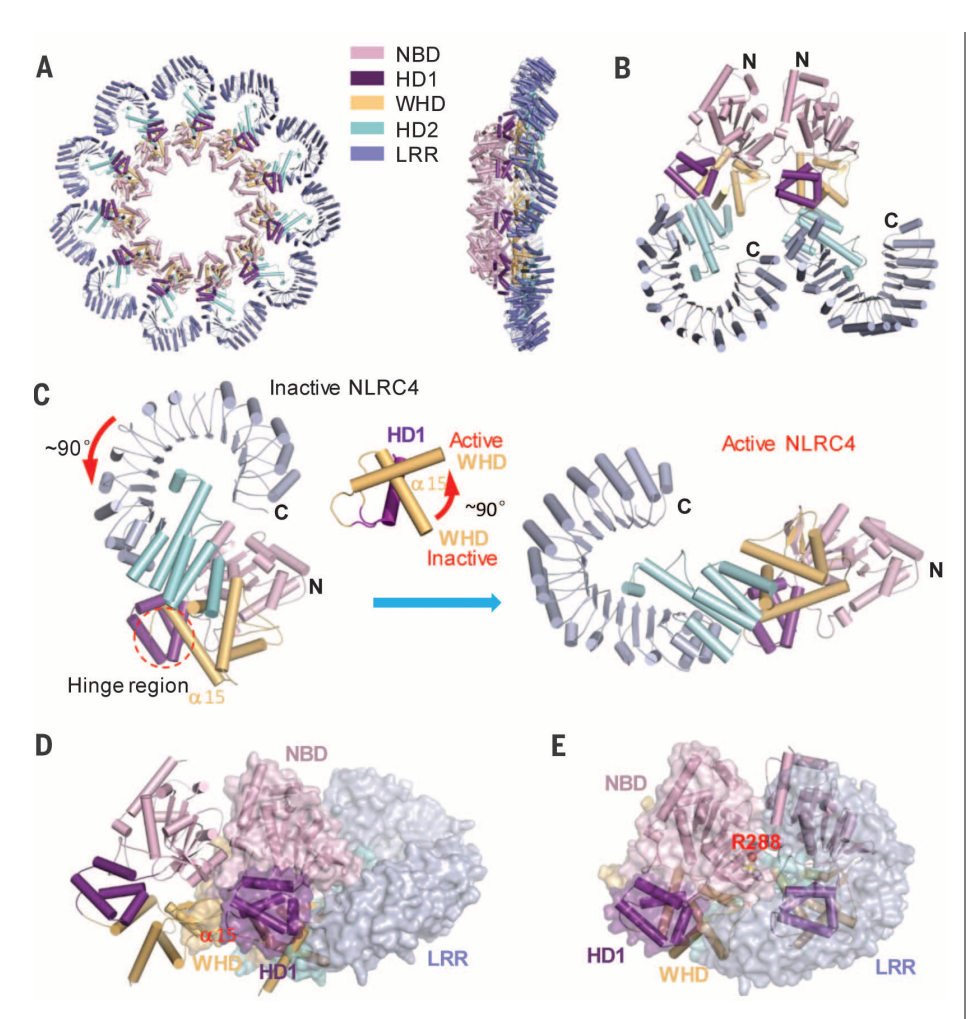


Fig. 2. NLRC4 activation creates the catalytic surface for oligomerization. (A) Cartoon representations of oligomerized NLRC4^{ACARD} in top and side views. Color codes for domains of NLRC4 are indicated. **(B)** A lateral dimer of NLRC4^{ACARD}. The N- and C-terminal sides of NLRC4 are labeled. **(C)** Striking structural reorganization occurs to NLRC4 during activation. Cartoon representations of the inactive (left) and active (right) structures of NLRC4. The two structures superimposed with the NOD module of the inactive NLRC4 as the template are shown in the same orientation. The red arrow indicates the direction of the C-terminal LRR domain movement from inactive to active state. The hinge region is highlighted in the red circle. The middle panel illustrates a structure comparison of the hinge region from the inactive and active structure. **(D)** The NOD module of the inactive NLRC4 (in transparent surface) was aligned with one NLRC4 monomer (right) from a lateral dimer (in cartoon). **(E)** The NOD module of the inactive NLRC4 (in transparent surface) was aligned with one NLRC4 monomer (left) from a lateral dimer (in cartoon).

this conclusion, NLRC4^{R288A} from the catalytic surface still displayed flagellin-induced interaction with NAIP5 but failed to form higher-order oligomeric complexes (*13*). Gel filtration analysis and negative staining EM 3D reconstruction showed that the flagellin-NAIP5-NLRC4^{R288AACARD} complex was dimeric in solution (Fig. 3C; fig. S12, A to E; and table S1). The 3D reconstruction (Fig. 3D) revealed a region of extra density for one of the two protomers, which is probably from NAIP5.

NLRC4^{L435DACARD} located at the same side as NLRC4^{R288AACARD} (Fig. 3B) generated similar effects on flagellin-induced NLRC4 oligomerization and interaction with NAIP5 (Fig. 3, C and E). Consistently, NLRC4^{L435D} and NLRC4^{Q433A} but not NLRC4^{R285A} and NLRC4^{R434A} abrogated flagellin-NAIP5 or PrgJ-NAIP2 mediated production of

IL-1 β , phenocopying NLRC4^{R288A} (fig. S13, A and B). Further supporting these results, NLRC4^{R285A Δ CARD} and NLRC4^{R434 Δ CARD} interacted with NAIP5 in a stoichiometry similar to the wild NLRC4^{ACARD} but different from NLRC4^{R288 Δ ACARD}, NLRC4^{L435D Δ CARD}, and NLRC4^{Q433 Δ ACARD} (Fig. 3E and fig. S14).

Asp¹²⁵ from the receptor surface was modeled to form polar interactions with Arg²⁸⁸ (Fig. 3B) from the catalytic surface. Consistently, NLRC4^{D125A} abrogated flagellin-NAIP5 or PrgJ-NAIP2 mediated generation of IL-1β (fig. S13, C and D). Similar results were obtained with the mutants NLRC4^{D123A} and NLRC4^{D124D} (Fig. 3B) located at the same oligomeric surface. However, a higher level of NLRC4^{D123A} protein was still responsive to flagellin or PrgJ (fig. S13, C and D), indicating

that this mutation only partially inhibited NLRC4 activation. NLRC4 $^{\rm ID4DACARD}$ and NLRC4 $^{\rm D125AACARD}$ displayed no detectable interaction with NAIP5 induced by flagellin in our pull-down assay (Fig. 3E), in sharp contrast with NLRC $^{\rm L435DACARD}$ and NLRC4 $^{\rm R288AACARD}$ from the catalytic surface (Fig. 3, C and E).

Our model (Figs. 3A and 4A) predicts that an activated NAIP or NLRC4 molecule can interact with and activate the inactive mutant NLRC4R288A that has an intact receptor surface. The NLRC4 mutant, however, is unable to activate a second inactive NLRC4 molecule due to its impaired catalytic surface. Thus, NLRC4^{R288A} is expected to inhibit formation of the wheel-like structure of the PrgJ-NAIP2-NLRC4FL complex by terminating the propagation of NLRC4, forming partially oligomerized structures. Indeed, the complex containing the four proteins was shifted to the lower molecular weight species as compared with the PrgJ-NAIP2-NLRC4^{FL} complex (Fig. 4B). As predicted, structures similar to those of the partially oligomerized PrgJ-NAIP2-NLRC4^{ΔCARD} were observed in the NLRC4^{R288AΔCARD}-containing complex (Fig. 4C). In further support of our model (Fig. 3A and fig. S15A), the constitutively active mutant NLRC4H443LACARD (13) interacted with and induced oligomerization of wild-type NLRC4^{FL} (fig. S15, B to E).

NAIPs possess catalytic surfaces matching the receptor surface of NLRC4

Our data (Figs. 1E, 3D, and 3E) support the idea that NAIP5 interacts with the receptor surface of NLRC4 (Fig. 5A). Well agreeing with this conclusion, Arg^{288} and the β -hairpin tip of WHD from the catalytic surface of NLRC4 are highly conserved in the NAIP members (Fig. 5B). In contrast, the critical amino acids from the receptor surface of NLRC4 are highly variable in all the NAIP members (Fig. 5B). Further supporting our model (Fig. 5A), mutations of Arg⁵⁹⁰ (Arg⁵⁹⁰Ala) and Leu⁷³⁷ (Leu⁷³⁷Asp) from NAIP5 or Arg⁶³⁴ (Arg⁶³⁴Ala) and Leu⁷⁸⁰ (Leu⁷⁸⁰Asp) from NAIP2 that are equivalents of Arg²⁸⁸ and Leu⁴³⁵ of NLRC4, respectively (Fig. 5B), resulted in no detectable activity of NLRC4-mediated production of IL-1ß (fig. S16, A and B). Substantial increases in protein expression, however, resulted in partial activity of the NAIP5 or NAIP2 mutants in producing IL-1ß (fig. S16, A and B). Interestingly, the two NAIP5 mutations were less effective in inhibiting flagellin-induced NAIP5-NLRC4 $^{\Delta CARD}$ interaction (Fig. 5C, top panel) than those from the receptor surface of NLRC4 (Fig. 3E). The reason for this might be that the residual activity of these NAIP5 mutant proteins still activated a small amount of NLRC4 that can proceed with autocatalytic activation. This differs from the mutations from the receptor surface that have an accumulating effect on inhibiting the assembly of NAIP-NLRC4 inflammasomes. Supporting these ideas, the two NAIP5 mutants exhibited nearly no detectable flagellin-induced interaction with NLRC4^{R288AΔCARD} (Fig. 5C, bottom panel) that has an impaired catalytic surface. By contrast, the immunoactive mutants NAIP5^{R587A} and NAIP5^{Q735A}

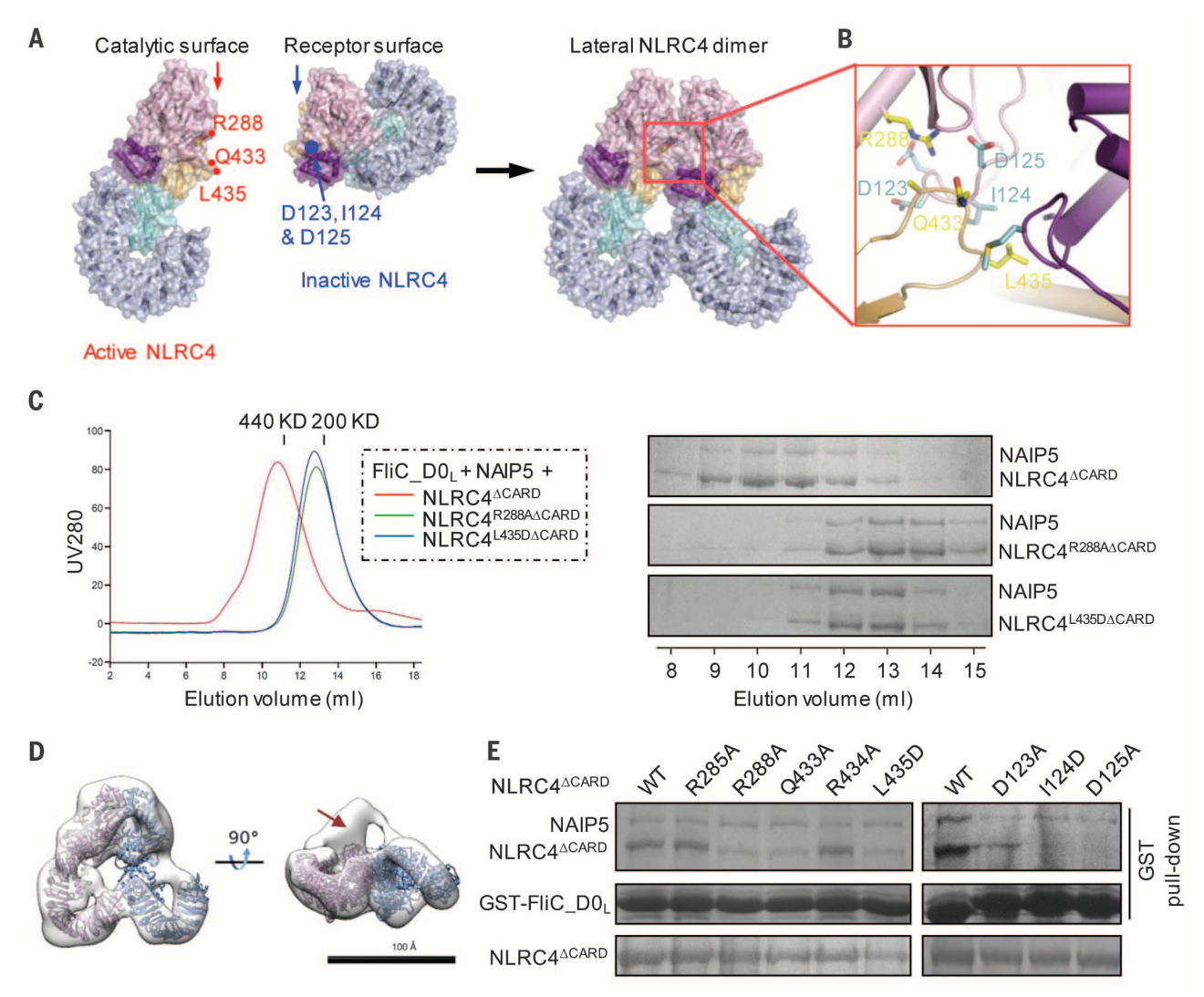


Fig. 3. The catalytic surface initiates NLRC4 self-oligomerization. (A) A model depicting formation of a lateral NLRC4 dimer through the interaction of an activated NLRC4 and with an inactive NLRC4. The red and blue arrows indicate the catalytic surface (in active NLRC4) and receptor surface, respectively. Positions of some residues from the catalytic surface and receptor surface are indicated. (B) Amino acids located at a lateral NLRC4 dimeric interface. Residues from the catalytic surface and receptor surface are colored in yellow and cyan, respectively. (C) GST-FliC_DO_L, NAIP5, and NLRC4 $^{\Delta CARD}$ wild type or mutants as indicated were coexpressed in insect cells, and the purified proteins were subjected to gel filtration analysis after removal of

glutathione S-transferase (GST). (Left) Gel filtration profiles of protein complexes as indicated. (Right) Samples of peak fractions shown in the left panel were visualized by Coomassie staining after SDS–polyacrylamide gel electrophoresis (SDS-PAGE). (\mathbf{D}) Surface representation of 3D reconstruction of the FliC_D0_L-NAIP5-NLRC4^{RZ88AΔCARD} complex shown in (C), with two NLRC4^{ΔCARD} monomers docked. The red arrow indicates the extra density map in which NLRC4^{ΔCARD} cannot be fitted. (\mathbf{E}) GST-FliC_D0_L, NAIP5, and wild-type NLRC4^{ΔCARD} or its mutants as indicated were coexpressed in insect cells. The proteins were purified using GS4B resin. Proteins bound to the resin were detected by Coomassie blue staining after SDS-PAGE.

displayed similar interactions with either wild-type $NLRC4^{ACARD}$ or $NLRC4^{R288AACARD}$ as compared with the wild-type NAIP5.

Together, our data showed that NAIP members do not possess a receptor surface matching the conserved catalytic surface of their own or NLRC4's, thus precluding them from self-oligomerization and further recruitment into an existing NAIP-NLRC4-containing complex by an activated NLRC4. These ensure incorporation of a single NAIP molecule into one NAIP-NLRC4 inflammasome.

Discussion

Our present study, together with others (33, 34), supports a sequential ligand-induced assembly of

NAIP-NLRC4 inflammasomes (fig. S17). The partially exposed receptor surface in the inactive NLRC4 (Figs. 2D and 3A) may adopt a metastable active state that has a higher binding affinity with the catalytic surface of an activated NLRC4. This interaction might also involve an induced-fit mechanism. Regardless of conformational selection or induced fit or both pathways, to avoid the clashes between the β -hairpin tip of WHD from an activated NLRC4 and the receptor surface of an inactive NLRC4 (Fig. 2D and fig. S11), their interaction may induce a concerted reorientation of the WHD from the inactive NLRC4 (Fig. 2C and fig. S9). This results in NLRC4 activation and formation of the catalytic

surface that activates a second inactive NLRC4 molecule, thus self-propagating the active conformation of NLRC4 to assemble the wheel-like structure of inflammasomes (fig. S17). Apaf-1 likely follows a different paradigm for oligomerization. Cryo-EM studies clearly showed a 1:1 stoichiometry between Apaf-1 and cytochrome c in apoptosome (28), suggesting that each Apaf-1 molecule needs activation by cytochrome c for oligomerization. This is supported by the observation that both of the two oligomerization surfaces of inactive Apaf-1 are completely buried (fig. S8C), ruling out the possibility of self-propagation.

The properties of NLRC4 oligomerization are reminiscent of the replication mechanism of a

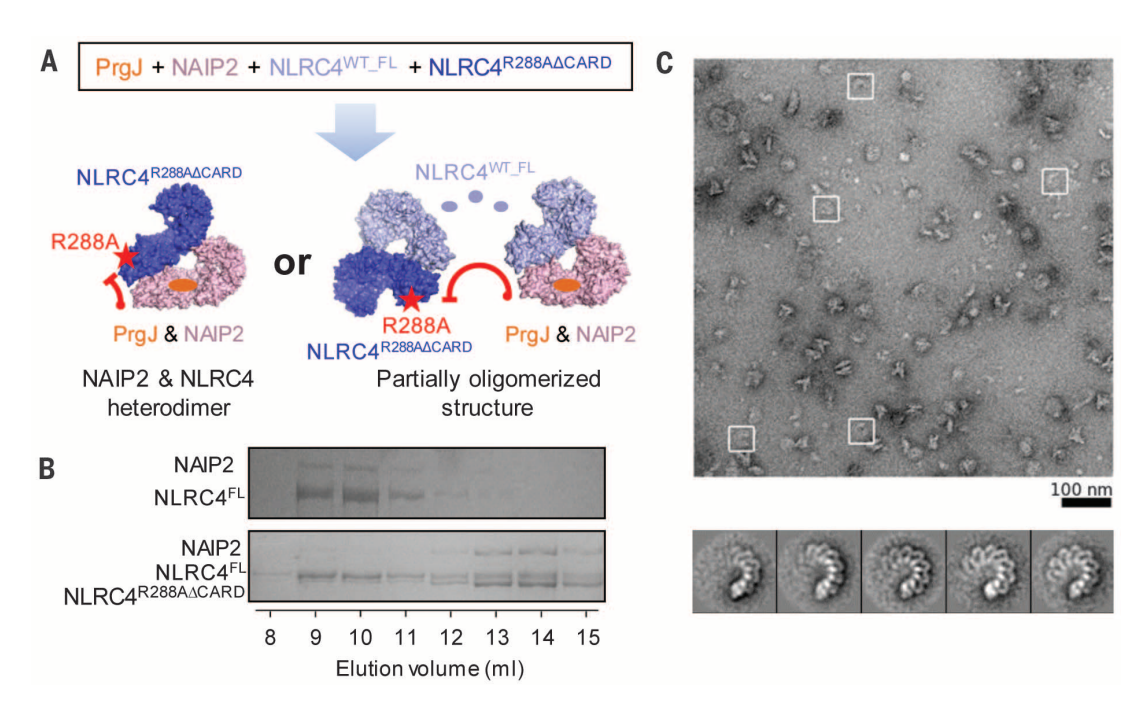


Fig. 4. NLRC4 is activated in a self-propagated manner. (**A**) A cartoon illustrating inhibition of the wheel-like structure of the PrgJ-NAIP2-NLRC4^{FL} complex by the mutant protein NLRC4^{R288AACARD}. The red star represents the position of Arg²⁸⁸Ala mutation from the catalytic surface. (**B**) Gel filtration analysis of the PrgJ-NAIP2-NLRC4^{FL} and PrgJ-NAIP2-NLRC4^{FL}-NLRC4^{R288AACARD} complexes. The peak fractions were visualized by SDS-PAGE with Coomassie blue staining. (**C**) Partially oligomerized structures of the PrgJ-NAIP2-NLRC4^{FL}-NLRC4^{R288AACARD} complex [sample from elution volume of 11 ml in (B)]. (Top) A representative negative-stain micrograph of the complex. (Bottom) Representative 2D class averages of the complexes.

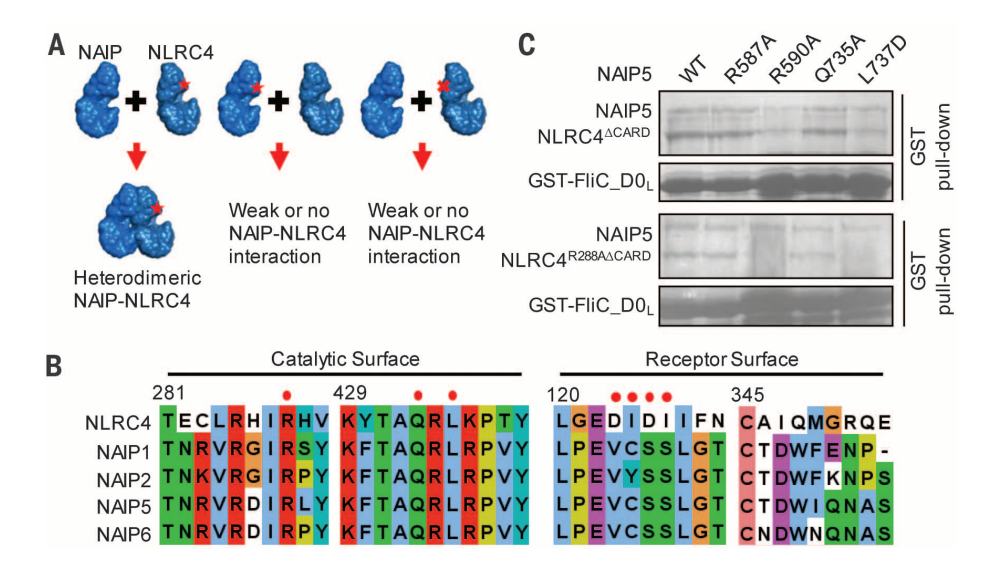


Fig. 5. NAIP members have a conserved catalytic surface with NLRC4. (A) A cartoon showing effects of mutations from NAIP or NLRC4 on their ligand-induced interaction. The red star and the red cross indicate mutations of key amino acids in the catalytic and receptor surface, respectively. (B) Sequence alignment of NAIP members with NLRC4 around the catalytic and receptor surface of NLRC4. The red dots on the top indicate the amino acids whose mutations disrupt or compromise formation of the wheel-like structures of NAIP-NLRC4 complexes. Numbers indicate the

positions of NLRC4 residues. Single-letter abbreviations for the amino acid residues are as follows: A, Ala; C, Cys; D, Asp; E, Glu; F, Phe; G, Gly; H, His; I, Ile; K, Lys; L, Leu; M, Met; N, Asn; P, Pro; Q, Gln; R, Arg; S, Ser; T, Thr; V, Val; W, Trp; and Y, Tyr. (\mathbf{C}) GST-FliC_DO_L, wild-type NAIP5 or its mutants, and wild-type NLRC4^CARD or NLRC4R288AACARD as indicated were coexpressed in insect cells. The proteins were purified using GS4B resin. Proteins bound to the resin were detected by Coomassie blue staining after SDS-PAGE.

prion in which conformational conversion from its properly folded isoform into the prion form (misfolded) is propagated in an autocatalytic manner (35). Such a mechanism would render the gain-of-function mutations mapped to destabilize the inactive conformation of NLRC4 (36–38) more efficient to induce NLRC4 activation. However, self-propagation of NLRC4 differs from that of a canonical prion in that the former is initiated by the PAMP-activated

NAIPs rather than self-seeded. Furthermore, self-propagation of NLRC4 leads to a soluble wheel-like structure with finite copies, whereas replication of a prion is self-perpetuating and thus results in formation of insoluble aggregates. Nonetheless,

the homologies between NLRC4 oligomerization and prion replication may help to better understand their underlying mechanisms. It remains unknown whether the prion-like mechanism is conserved in other immune NLR sensors for oligomerization. However, one apparent advantage of this mechanism is that a single PAMP or a host-derived danger molecule is sufficient for inducing formation of a fiber assembly, which in principle contains endless ASC because of its self-perpetuation property (39) and thus generates an all-or-none response (40). The requirement of ligand for initiation of this activity could serve to minimize inadvertent activation of an NLR protein through intermolecular collisions.

REFERENCES AND NOTES

- 1. K. Schroder, J. Tschopp, Cell 140, 821-832 (2010).
- L. Franchi, R. Muñoz-Planillo, G. Núñez, Nat. Immunol. 13, 325–332 (2012).
- V. A. Rathinam, S. K. Vanaja, K. A. Fitzgerald, *Nat. Immunol.* 13, 333–342 (2012).
- J. von Moltke, J. S. Ayres, E. M. Kofoed, J. Chavarría-Smith, R. E. Vance, Annu. Rev. Immunol. 31, 73–106 (2013).
- B. K. Davis, H. Wen, J. P. Ting, Annu. Rev. Immunol. 29, 707–735 (2011).
- M. Lamkanfi, V. M. Dixit, Annu. Rev. Cell Dev. Biol. 28, 137–161 (2012).
- T. Strowig, J. Henao-Mejia, E. Elinav, R. Flavell, *Nature* 481, 278–286 (2012).
- 8. H. Wen, J. P. Ting, L. A. O'Neill, *Nat. Immunol.* **13**, 352–357
- F. Martinon, K. Burns, J. Tschopp, Mol. Cell 10, 417–426 (2002).
- O. Danot, E. Marquenet, D. Vidal-Ingigliardi, E. Richet, Structure 17, 172–182 (2009).
- 11. N. Yan, Y. Shi, Annu. Rev. Cell Dev. Biol. 21, 35–56
- W. Chuenchor, T. Jin, G. Ravilious, T. S. Xiao, *Curr. Opin. Immunol.* 26, 14–20 (2014).
- 13. Z. Hu et al., Science 341, 172-175 (2013).
- 14. X. Cai et al., Cell 156, 1207-1222 (2014).
- 15. A. Lu et al., Cell 156, 1193-1206 (2014).
- 16. L. Franchi et al., Nat. Immunol. 7, 576-582 (2006).
- 17. K. L. Lightfield *et al.*, *Nat. Immunol.* **9**, 1171–1178 (2008).
- 18. E. A. Miao et al., Nat. Immunol. 7, 569-575 (2006).
- E. A. Miao et al., Proc. Natl. Acad. Sci. U.S.A. 107, 3076–3080 (2010).
- A. B. Molofsky et al., J. Exp. Med. 203, 1093–1104 (2006).
- T. Ren, D. S. Zamboni, C. R. Roy, W. F. Dietrich, R. E. Vance, *PLOS Pathog.* 2, e18 (2006).
- 22. F. S. Sutterwala *et al.*, *J. Exp. Med.* **204**, 3235–3245 (2007).
- J. Yang, Y. Zhao, J. Shi, F. Shao, Proc. Natl. Acad. Sci. U.S.A. 110, 14408–14413 (2013).
- 24. E. M. Kofoed, R. E. Vance, Nature 477, 592-595 (2011).
- 25. Y. Zhao et al., Nature 477, 596-600 (2011).
- J. L. Tenthorey, E. M. Kofoed, M. D. Daugherty, H. S. Malik, R. E. Vance, *Mol. Cell* 54, 17–29 (2014).
- 27. E. F. Halff et al., J. Biol. Chem. **287**, 38460–38472 (2012).
- S. Yuan, M. Topf, T. F. Reubold, S. Eschenburg, C. W. Akey, Biochemistry 52, 2319–2327 (2013).
- 29. S. Yuan et al., Structure **19**, 128–140 (2011).
- 30. Y. Pang et al., Genes Dev. 29, 277-287 (2015).
- 31. S. Qi et al., Cell 141, 446-457 (2010).
- T. F. Reubold, S. Wohlgemuth, S. Eschenburg, Structure 19, 1074–1083 (2011).
- 33. R. E. Vance, Curr. Opin. Immunol. 32, 84–89 (2015).
- 34. L. Zhang et al., Science 350, 404-409 (2015).
- P. Chien, J. S. Weissman, A. H. DePace, *Annu. Rev. Biochem.* 73, 617–656 (2004).
- 36. S. W. Canna et al., Nat. Genet. **46**, 1140–1146 (2014).
- 37. N. Romberg et al., Nat. Genet. 46, 1135-1139 (2014).

- A. Kitamura, Y. Sasaki, T. Abe, H. Kano, K. Yasutomo, J. Exp. Med. 211, 2385–2396 (2014).
- X. Cai, Z. J. Chen, Trends Immunol. 35, 622–630 (2014).
 Q. Yin, T. M. Fu, J. Li, H. Wu, Annu. Rev. Immunol. 33, 393–416 (2015).

ACKNOWLEDGMENTS

We thank Y. Xu and T. Yang at Tsinghua University Branch of China National Center for Protein Sciences Beijing for data collection and computational support, and X. Li for technical instructions of using the K2-Summit camera. We acknowledge the computational facility support on the Explorer 100 cluster system of Tsinghua National Laboratory for Information Science and Technology. The data presented in this paper are tabulated in the main paper and in the supplementary materials. The EM maps have been deposited in the Electron Microscopy Data Bank with accession codes EMD-3139/3140 for the 12- or 11-protomer PrgJ-NAIP2-NLRC4^{TC} complex, EMD-3141/3142 for the 11- or 10-protomer PrgJ-NAIP2-NLRC4^{ACARD} complex, and EMD-3143 for the

FliC_DO_L-NAIP5-NLRC4^{R288AACARD} complex. This research was funded by the Chinese Ministry of Science and Technology (2014CB910101 to J.C., 2011CB910501 to S.-F.S., and 2012CB917303 to H.-W.W.) and the National Natural Science Foundation of China (31230016 to S.-F.S.). Z.H. was supported by a China Postdoctoral Science Foundation-funded project and the Center for Life Sciences (CLS) Postdoctoral Fellowship Foundation. Q.Z. was supported by the CLS Postdoctoral Fellowship Foundation.

SUPPLEMENTARY MATERIALS

www.sciencemag.org/content/350/6259/399/suppl/DC1 Materials and Methods Figs. S1 to S18 Table S1 References (41–56)

11 May 2015; accepted 14 September 2015 Published online 8 October 2015 10 1126/science aac5489

REPORTS

INNATE IMMUNITY

Cryo-EM structure of the activated NAIP2-NLRC4 inflammasome reveals nucleated polymerization

Liman Zhang, \$^{1,2*}\$ Shuobing Chen, \$^{3,4*}\$ Jianbin Ruan, \$^{1,2}\$ Jiayi Wu, \$^{3,4}\$ Alexander B. Tong, \$^{1,2}\$ Qian Yin, \$^{1,2}\$ Yang Li, \$^{1,2}\$ Liron David, \$^{1,2}\$ Alvin Lu, \$^{1,2}\$ Wei Li Wang, \$^{4,5}\$ Carolyn Marks, \$^6\$ Qi Ouyang, \$^3\$ Xinzheng Zhang, \$^7\$ Youdong Mao, \$^{3,4,5}\$ \dagger Hao Wu 1,2 \dagger

The NLR family apoptosis inhibitory proteins (NAIPs) bind conserved bacterial ligands, such as the bacterial rod protein PrgJ, and recruit NLR family CARD-containing protein 4 (NLRC4) as the inflammasome adapter to activate innate immunity. We found that the PrgJ-NAIP2-NLRC4 inflammasome is assembled into multisubunit disk-like structures through a unidirectional adenosine triphosphatase polymerization, primed with a single PrgJ-activated NAIP2 per disk. Cryo-electron microscopy (cryo-EM) reconstruction at subnanometer resolution revealed a ~90° hinge rotation accompanying NLRC4 activation. Unlike in the related heptameric Apaf-1 apoptosome, in which each subunit needs to be conformationally activated by its ligand before assembly, a single PrgJ-activated NAIP2 initiates NLRC4 polymerization in a domino-like reaction to promote the disk assembly. These insights reveal the mechanism of signal amplification in NAIP-NLRC4 inflammasomes.

he nucleotide-binding domain (NBD) and leucine-rich repeat (LRR)-containing protein (NLR) family participates in the formation of inflammasomes that activate caspase-1 for cell death induction and cytokine maturation. NLR family apoptosis inhibitory proteins (NAIPs) are so far the only NLR family members with specifically defined ligands (1-4). NAIP2 detects the inner rod protein of the bacterial type III secretion system, including Salmonella typhimurium PrgJ, whereas NAIP5 and NAIP6 detect bacterial flagellin such as Salmonella typhimurium FliC (2, 4, 5). NLR family caspase recruitment domain (CARD)containing protein 4 (NLRC4) was initially found to participate in caspase-1 activation and inter-

leukin (IL)– 1β secretion in response to cytoplasmic flagellin (6) and was only recently shown to be the common adapter for NAIPs (2, 4). The NAIP-NLRC4 inflammasomes perform effector functions against intracellular bacteria (7, 8), play protective roles in mouse models of colitisassociated colorectal cancer (9, 10), and serve as a potential strategy in tumor immunotherapy (11). Mutations in NLRC4 also induce auto-inflammatory diseases in humans (10, 12–14).

We assembled the FliC-activated NAIP5-NLRC4 complex and the PrgJ-activated NAIP2-NLRC4 complex with the use of CARD-deleted NLRC4 (NLRC4 \triangle) to avoid potential CARD-mediated aggregation (Fig. 1A). Either full-length NAIP2 or N-terminal baculovirus inhibitor of apoptosis protein repeat





Structural and biochemical basis for induced self-propagation of NLRC4

Zehan Hu *et al.* Science **350**, 399 (2015); DOI: 10.1126/science.aac5489

This copy is for your personal, non-commercial use only.

If you wish to distribute this article to others, you can order high-quality copies for your colleagues, clients, or customers by clicking here.

Permission to republish or repurpose articles or portions of articles can be obtained by following the guidelines here.

The following resources related to this article are available online at www.sciencemag.org (this information is current as of October 26, 2015):

Updated information and services, including high-resolution figures, can be found in the online version of this article at:

http://www.sciencemag.org/content/350/6259/399.full.html

Supporting Online Material can be found at:

http://www.sciencemag.org/content/suppl/2015/10/07/science.aac5489.DC1.html

A list of selected additional articles on the Science Web sites **related to this article** can be found at:

http://www.sciencemag.org/content/350/6259/399.full.html#related

This article **cites 55 articles**, 8 of which can be accessed free: http://www.sciencemag.org/content/350/6259/399.full.html#ref-list-1

This article has been **cited by** 1 articles hosted by HighWire Press; see: http://www.sciencemag.org/content/350/6259/399.full.html#related-urls